Electrochemical Characterization of Manganese Oxide Cathode Materials based on $Na_{0.4}MnO_2$

Felix Hu and Marca M. Doeff*

Materials Sciences Division, Lawrence Berkeley National Laboratory, University of California at Berkeley, Berkeley, CA 94720, USA.

*Corresponding author: mmdoeff@lbl.gov

Abstract

Cathode materials for lithium rechargeable batteries were prepared from $Na_{0.4}MnO_2$ by solution and molten salt ion-exchanges. The former process results in partial replacement of sodium while the latter results in complete exchange. The discharge characteristics depend upon the sodium content, with the partially lithiated material exhibiting hysteresis in the charge/discharge profile and differential capacity plots from stepped potential experiments. For the fully lithiated material, a complex voltage profile with several distinct plateaus corresponding to several two-phase regions is observed. No evidence of spinel formation during ion exchange or electrochemical cycling is seen for this system.

Keywords: manganese oxide, rechargeable lithium batteries, romanechite

Introduction

Manganese oxides are attractive replacements for the currently used cobalt oxide electrodes[1, 2] used in commercial lithium ion batteries, because of the potential for lower cost and improved safety in such devices. Many different manganese oxide structures exist, but the most widely studied materials for this application are those related to the spinel, $LiMn_2O_4$.[3] Recently, several compounds in the Na-Mn-O system [4] have been investigated, including those containing tunnels [5, 6, 7, 8] or with layered arrangements [9, 10, 11, 12] not available directly in the Li-Mn-O system. In general, these are ion-exchanged prior to fabrication into electrodes to avoid complications arising from the presence of sodium ions in lithium cells, such as plating of sodium metal on the anode. The resultant products are meta-stable; thus, it is important to evaluate their tendencies to convert into more stable phases, such as spinel, during normal and abusive cell operation conditions. In general, tunnel compounds require more rearrangement to convert to spinel than layered compounds that have nearly cubic close packing of oxygen ions, making them more resistant to phase conversion. (Layered compounds with different oxygen arrays also appear more resistant to phase conversion. [10, 12]) Tunnel compounds, however, are more likely to be site-limited than layered compounds, giving lower theoretical capacities. Hence, there appears to be a trade-off between high capacity and stable cycling for manganese oxide structures.

$Na_{0.4}MnO_2$ has been reported [13] to have the same structure as the barium-containing mineral, romanechite [14]; i.e., with tunnels three MnO_6 octahedra long and two octahedra wide (Figure 1a). A number of other tunnel-containing manganese oxides exist such as α-MnO_2 (2 x 2 tunnels) and todorokite (3 x 3 tunnels) [15]. Many of these

tunnel compounds can be synthesized from birnessite, a hydrated manganese oxide with a layered arrangement (Figure 1b), and, indeed, are structurally similar, with double or triple stacks of MnO_6 octahedra acting as pillars between birnessite-like layers. These tunnel compounds, are, therefore, interesting intermediate cases between the higher capacity layered structures and the more stable tunnel ones. Herein, we report our results on compounds derived from one of these, $Na_{0.4}MnO_2$.

Experimental

For synthesis of $Na_{0.4}MnO_2$, $NaNO_3$ and 47.5% $Mn(NO_3)_2$ in aqueous HNO_3 were mixed with glycine in the molar ratio 1:2 (glycine:nitrate) and diluted with de-ionized water. The solution was then combusted by dripping it slowly into a heated metal beaker.[16] The resultant powder was calcined at 600°C for 4h to remove any organic residue and to obtain a homogenous material.

For ion-exchange, some of the $Na_{0.4}MnO_2$ powder was refluxed in a solution of LiBr in ethanol (9 fold excess of Li) for 48h at 80°C. Another portion of $Na_{0.4}MnO_2$ was added to a mixture of 30 mol % $LiNO_3$ and 70 mol% $LiNO_2$ (5 fold excess of Li) and heated to 200˚C in a Teflon beaker. After 24 hrs, the molten salt was poured out and a fresh aliquot of the salt mixture was added. This was repeated once more, for a total heating time of 72 hours. Both of the ion-exchanged samples were washed thoroughly to remove the salts and dried at least 24 hours at 120˚C.

The structures of the as-made and ion-exchanged materials were identified using X-ray diffraction (XRD) on a Phillips X'pert diffractometer, with monochromized Cu radiation (λ = 1.54 Å). The elemental composition was determined by inductively coupled plasma (ICP) analysis performed by Desert Analytics Laboratory, Tucson, AZ.

Electrodes were prepared by thoroughly mixing 84 wt% active material with 4% carbon black (Shawinigan Black), 4% SFG-6 graphite (Timrex Timcal) and 8% PVdF (from a 6% NMP-solution) and extruding onto an aluminum-foil. Typical loadings were about 10-15 mg active material/cm^2. The electrodes were allowed to dry overnight at room temperature and for 24h at 120°C. Coin cells were assembled in a glove-box (<1 ppm O_2/H_2O) using Celgard 3401 as separator, ethylene-carbonate (EC)/dimethyl-carbonate (DMC) + 1M $LiPF_6$ electrolyte (Selectipur®, Merck, Darmstadt, Germany), and Li-foil (Cyprus-Foote Mineral Co., Kings Mountain, NC) as the counter electrode. A MacPile II (Bio-Logic, SA, Claix, France) was used for electrochemical testing. For the galvanostatic experiments, cells were cycled between set voltage limits with 15 minute rests between each half-cycle. For electrochemical potential spectroscopy experiments, 10 mV steps were taken every 4 hours, or after the current had decayed to 1/1000 of the initial value, whichever came first.

Results & Discussion

Elemental analyses on the as-made sample give a Na:Mn ratio of 0.41, close to the nominal composition of $Na_{0.4}MnO_2$. The composition of the solution exchanged material is $Na_{0.17}Li_{0.16}MnO_2$, indicating that slight oxidation of the sample took place as well as partial replacement of Na. Only a trace of sodium (less than 0.5%) was found in the molten salt exchanged material, which we will refer to as $Li_{0.4}MnO_2$ hereafter, for the sake of simplicity.

$Na_{0.4}MnO_2$ may be prepared from birnessite by heating [8] or directly by conventional solid state synthesis when the reaction temperature is below about 750˚ C. [13] In practice, it can be difficult to obtain pure materials by the latter method, because

of the existence of another line phase close in composition, $Na_{0.44}MnO_2$, with a different tunnel structure. The product composition in this study was very sensitive both to calcination temperature and to the Na:Mn ratio used in the precursor mix: above 600˚C, two-phase mixtures containing $Na_{0.44}MnO_2$ were frequently obtained, but even slight deficiencies in the precursor Na content gave Mn_2O_3 as an impurity. For a calcination temperature of 600˚C, nearly phase-pure $Na_{0.4}MnO_2$ could be reliably prepared, although the results were still very dependent upon the precursor Na:Mn ratio, with changes as small as 0.05 resulting in large increases in amounts of secondary phases.

An XRD pattern of $Na_{0.4}MnO_2$ is shown in Figure 2. Agreement between the experimental patterns for this $Na_{0.4}MnO_2$ and those previously reported [8, 13] is nearly exact. We could not, however, satisfactorily reproduce the pattern using the lattice parameters reported in reference 13 and the C12/m1 space group and atom positions reported for romanechite, [14] although $Na_{0.4}MnO_2$ appears to be structurally related. It is possible that the unit cell parameters previously reported are incorrect, or that $Na_{0.4}MnO_2$ belongs to a different space group or has a more complex structure (such as tunnels of varying sizes). Several other manganese oxides with complex XRD patterns have been found to contain two or more types of tunnels with differing dimensions; e.g., γ-MnO_2 with 2 x 1 and 1 x 1 tunnels [17] and hollandite/romanechite intergrowths with 2 x 2 and 2 x 3 tunnels [18]. In the absence of more structural information, such as that obtained from single crystal data, it is not possible to distinguish between these possibilities or refine the pattern satisfactorily. Transmission electron microscopy experiments on this material are planned in the near future to elucidate the structure.

Figure 2 also shows patterns of the partially and fully ion-exchanged materials. The lithiated phases appear to be structurally related to $Na_{0.4}MnO_2$, but the peaks are shifted. This is particularly evident at low angles (see inset), and is more pronounced for $Li_{0.4}MnO_2$ than for $Na_{0.17}Li_{0.16}MnO_2$. This is consistent with retention of the $Na_{0.4}MnO_2$ structure with decreases in the unit cell parameters due to replacement of sodium with smaller lithium ions. Notably, the patterns of the exchanged materials do not bear a resemblance to that of a lithium manganese oxide spinel phase, and the intense spinel 311 reflection at $2\theta = 36.2^\circ$ (d = 2.48) is absent indicating that spinel is not present as a minor phase.

$Li/Na_{0.17}Li_{0.16}MnO_2$ cells are in the partially discharged state when assembled and may either be charged or discharged initially. Figure 3 shows the initial galvanostatic partial charge to 4.5V and first discharge to 2.8V of a typical cell and Figure 4 shows a differential capacity plot obtained from a stepped potential experiment. A composition of approximately $(Li, Na)_{0.07}MnO_2$ is reached when the cell is charged to 4.5V, indicating that some sodium ions as well as lithium ions are de-intercalated. Considerable hysteresis is seen both in the cycling profile and in the differential capacity plot, with main features (peaks or plateaus) evident at 3.67, 2.96 and 2.65V during discharge and 3.66, 3.63, 3.14 and 3.02V during charge. The hysteresis is somewhat reproducible from cycle to cycle if the discharge voltage is limited to 2.5V or higher (x in $(Li,Na)_xMnO_2 \approx 0.6$). Discharges below this voltage result in rapid capacity fading, but fairly good cycling is obtained when higher voltage limits are used. (Figure 5).

The presence of mobile sodium ions in the active material and cells makes it difficult to interpret the electrochemical behavior. For example, sodium will plate before

lithium on the negative electrode during charge and may affect the cell potential. Diffusion rates for sodium and lithium ions are likely to be different, and the presence of sodium ions in partially filled tunnels may influence the availability of sites for lithium and give rise to the observed hysteresis.

Complications from sodium are avoided in the $Li/Li_{0.4}MnO_2$ cells. Figure 6 shows stepped potential experiments on two different cells, one started on charge and the second started on discharge. The first cycle for both was between 2.8 and 3.9V, and both show a prominent, reversible set of peaks centered at about 3.7V vs. Li. When the potential limit is increased (Figure 6a), two additional sets of features are observed at about 4.02V and above 4.2V. These show a time-dependent quasi-reversibility; i.e., the magnitudes of correlated peaks on the discharge traces are dependent upon the amount of time between half-cycles, and the cell potential drops upon rest, although the peak at 3.7V is not affected, and the features re-appear upon re-charge. This suggests that a fairly rapid self-discharge process is occurring. For the cell discharged to 2.5V (Figure 6b), a large peak is observed at 2.8V and is associated with the 3.1V feature observed upon subsequent charge. (This is also evident in later cycles in the data shown for Figure 6a, although less pronounced).

Figure 7 shows the pseudo-open circuit profile obtained by integrating the differential capacity data obtained on the cell shown in Figure 6b. The peaks at 2.8/3.1V in the differential capacity plot correspond to a long plateau starting at a composition of about $x = 0.5$ in Li_xMnO_2, and discharging into this region results in capacity loss, as can be seen in the third cycle in Figure 7. This is reminiscent of the behavior of a manganese oxide spinel, which also has capacity above 4V (often divided into two smaller plateaus)

like this material. The plateau at 3.7V is not typical of spinels, however, and is unaffected by cycling below 2.8V and above 3.9V. This suggests that conversion to spinel is not occurring.

Several cells were slowly charged or discharged to set voltage limits and disassembled. XRD patterns were obtained on the electrodes from these cells and are shown in Figures 8 and 9, along with that of the starting material in powder form ($Li_{0.4}MnO_2$, 3.3V vs. Li). The patterns of the charged and discharged electrodes are similar to that of $Li_{0.4}MnO_2$, although many peaks are shifted and some are split or have coalesced with others. Significantly, none resemble that of lithium manganese oxide spinel, and none of the reflections can be conclusively assigned to a spinel phase. Electrodes deeply discharged twenty times or more dramatically lose capacity and many of the voltage profile features, but still give XRD patterns resembling those presented in these figures, although peak breadths increase markedly and the intensities decrease, implying a loss of crystallinity.

The complexity of the patterns and the lack of structural information for these materials make interpretation difficult except in a general sense. For XRD patterns having many overlapping reflections, the shifts of peaks caused by changes in the unit cell parameters during intercalation/de-intercalation may cause apparent splitting (or coalescence), which can be misinterpreted as growth (or disappearance) of a second phase. For these materials, there are few reflections at very low angles (below $2\theta = 10^{\circ}$), so splitting of peaks can more confidently be associated with the coexistence of two phases. This is clearly seen in Figure 9 for the electrode charged to 3.75V. These two phases have approximate compositions of $Li_{0.26}MnO_2$ and $Li_{0.4}MnO_2$ based on the

electrochemical data (endpoints of the plateau centered at about 3.7V), and appear to be structurally related. The pattern for the electrode discharged to the middle of the plateau at 2.8V is more ambiguous, although the presence of many split peaks between $2\theta = 15^{\circ}$ and 20°, and the electrochemical behavior in this region imply the coexistence of two related phases, $Li_{0.5}MnO_2$ and $Li_{0.75}MnO_2$. It is interesting to note that the filling by lithium of all four corner sites in the 2 x 3 tunnels in a romanechite-type structure would lead to a formula of $Li_{0.8}MnO_2$ [19], close to the endpoint obtained during the electrochemical experiments and the composition of one of the phases associated with the 2.8V plateau.

Although $Li_{0.4}MnO_2$ does not readily convert to spinel during ion-exchange or redox processes, the cycling behavior is very sensitive to the conditions used. Good capacity retention is obtained only at low discharge rates when voltages are kept between 3.9 and 2.8V (Figure 10a), severely limiting utilization. Deep discharge into the 2.8V plateau results in rapid fading, suggesting that there are severe strains associated with the $Li_{0.5}MnO_2/Li_{0.75}MnO_2$ phase transition. Increasing the upper voltage limit upon charge results in higher discharge capacities, although this depends somewhat upon the amount of time spent on open circuit between half-cycles, due to the self-discharge previously described. There is also moderate capacity fading upon cycling (Figure 10b). It may, however, be possible to improve this by choosing cell components (e.g., electrolyte solutions) that are more resistant to oxidation; decomposition of these materials by the delithiated cathode material may cause increased cell impedance, leading to premature end-of-charge and apparent capacity loss.

$Li_{0.4}MnO_2$ shows electrochemical behavior that is intermediate between that of tunnel and layered manganese oxides. Like lithiated materials with the $Na_{0.44}MnO_2$ tunnel structure, [5, 7] it is meta-stable with respect to spinel conversion, although it does not show the same robustness and good cycling behavior. The theoretical capacity approaches that of the less spinel-conversion resistant layered compounds. Unfortunately, the steeply sloping discharge profile, sensitivity to deep discharge, and tendency to undergo self-discharge at high states-of-charge may mean that it will not be useful as a battery electrode, although other applications (such as sensors) may be possible.

Conclusions

$Na_{0.17}Li_{0.16}MnO_2$ and $Li_{0.4}MnO_2$ was prepared from $Na_{0.4}MnO_2$ by solution and molten salt exchanges, respectively. The lithiated materials appear to retain the structure of $Na_{0.4}MnO_2$ and do not convert to spinel upon cycling in lithium cells. Several features in the voltage profiles and differential capacity plots are observed. The electrochemical behavior of $Na_{0.17}Li_{0.16}MnO_2$ is complex and difficult to interpret due to the presence of mobile sodium ions. There is evidence for several distinct phases with approximate compositions $Li_{0.26}MnO_2$, $Li_{0.4}MnO_2$, $Li_{0.5}MnO_2$ and $Li_{0.75}MnO_2$ in the XRD and electrochemical data of cells containing the fully exchanged manganese oxide, although the exact structures of these phases is not known.

Acknowledgments

This work was supported by the Assistant Secretary for Energy Efficiency and Renewable Energy, Office of FreedomCAR and Vehicle Technologies of the U.S. Department of Energy under Contract No. DE-AC03-76SF00098.

References

[1] M. Winter, J.O. Besenhard, M.E. Spahr and P. Novak, Adv. Mater., 10 (1998) 725.

[2] J.M. Tarascon and M. Armand, Nature, 414 (2001) 359.

[3] M. M. Thackeray, Prog. Solid State Chem., 25 (1997) 1.

[4] M. M. Doeff, International Battery Association/Hawaii Battery Conference 2003, Waikoloa, HI, January 2003.

[5] M. M. Doeff, T. J. Richardson, and L. Kepley, J. Electrochem. Soc. 143 (1996) 2507).

[6] M. M. Doeff, T. J. Richardson, J.Hollingsworth, C. Yuan, and M. Gonzales, J. Power Sources 112/1 (2003) 294.

[7] M. M. Doeff, A. Anapolsky, L. Edman, T.J. Richardson and L.C. De Jonghe, J. Electrochem. Soc., 148 (2001) A230.

[8] M. Tsuda, H. Arai, Y. Nemoto and Y. Sakurai, J. Electrochem. Soc. 150 (2003) A659.

[9] A.R. Armstrong and P.G. Bruce, Nature, 381 (1996) 499.

[10] J.M. Paulsen, C.L. Thomas and J.R. Dahn, J. Electrochem. Soc., 146 (1999) 3560.

[11] T.A. Eriksson and M. M. Doeff, J. Power Sources**,** 119-120C (2003) 145.

[12] T. A. Eriksson, Y. J. Lee, J. Hollingsworth, J. A. Reimer, E. J. Cairns, X Zhang, and M. M. Doeff, Chem. Mater**.**, (2003) in press.

[13] J.-P. Parant, R. Olazcuaga, M. Devalette, C. Fouassier, and P. Hagenmuller, J. Solid State Chem. 3 (1971) 1.

[14] S. Turner and J. E. Post, Amer. Mineralogist, 73 (1988) 1155

[15] J. E. Post and D. L. Bish, Amer. Mineralogist, 73 (1988) 861.

[16] L.A. Chick, L.R. Pederson, G.D. Maupin, J.L. Bates, L.E. Thomas, G.J. Exarhos, Mater. Letters, 10 (1990) 6.

[17] Y. Chabre and J. Pannetier, Prog. Solid State Chem., 23 (1995) 1.

[18] S. Turner and P.R. Buseck, Science, 203 (1979) 456.

[19] A. Mendiboure, C. Delmas, and P. Hagenmuller, J. Sol. State Chem., 57 (1985) 323.

Figure Captions

Figure 1. a) Romanechite structure, looking down the b-axis. Spheres represent barium ions. B) birnessite structure, looking down the b-axis. Unit cells are marked with heavy gray lines.

Figure 2. XRD patterns for (bottom) $Na_{0.4}MnO_2$, (middle) $Na_{0.17}Li_{0.16}MnO_2$, the product of solution exchange, and (top) $Li_{0.4}MnO_2$, the product of molten salt exchange. The inset shows the low angle region expanded.

Figure 3. First partial charge and subsequent discharge of a Li/1M $LiPF_6$, EC-DMC/$Na_{0.17}Li_{0.16}MnO_2$ cell at 0.055 mA/cm^2 (approximately C/20).

Figure 4. Differential capacity plot obtained from a stepped potential experiment on a Li/1M $LiPF_6$, EC-DMC/$Na_{0.17}Li_{0.16}MnO_2$ cell. The potential was stepped 10 mV/4 hrs between 2.5 and 3.9V. The cell was initially stepped to 2.5V, then underwent a full cycle. The upper trace represents cell charge, and the lower cell discharge.

Figure 5. The first through 40th discharges of a Li/1M $LiPF_6$, EC-DMC/$Na_{0.17}Li_{0.16}MnO_2$ cell at 0.055 mA/cm^2. The 1st and 40th discharges are labeled, and every fifth discharge is shown from discharge 5 to 40.

Figure 6. Differential capacity plots obtained from stepped potential experiments for two Li/1M $LiPF_6$, EC-DMC/$Li_{0.4}MnO_2$ cells. a) cell was initially stepped to 2.8V, then cycled one cycle between 2.8 and 3.9V. The second full cycle was between 2.8 and 4.2V and the third was between 2.8 and 4.3V, b) cell was initially stepped to 3.9V, then cycled one full cycle between 2.8 and 3.9V. The second full cycle was between 2.5 and 3.9V and the third was between 2.5 and 4.3V. The potential was stepped 10 mV/4 hrs.

Figure 7. Pseudo-open circuit potential profiles obtained from integrating the data from the stepped potential experiments on the cell shown in Figure 7b; first cycle (—), second cycle (---), and third cycle (····).

Figure 8. (a) Charge/discharge profiles of Li/Li_xMnO_2 cells used for ex situ XRD experiments. Current density was 0.011 mA/cm^2 for all cells (approximately C/250). Squares mark where the ex situ measurements were made. (b) XRD patterns of electrodes from these cells. For the starting composition ($Li_{0.4}MnO_2$, 3.3V vs. Li), the powder was used rather than an electrode. Reflections from cell components are marked: G for graphite and Al for aluminum.

Figure 9. Low angle region of Figure 8b expanded.

Figure 10. Discharges of Li/1M $LiPF_6$, EC-DMC/$Li_{0.4}MnO_2$ cells at 0.011 mA/cm^2 between (a) 3.9 and 2.8V and (b) 4.5 and 2.8V. Cells spent 15 minutes on open circuit between half-cycles.

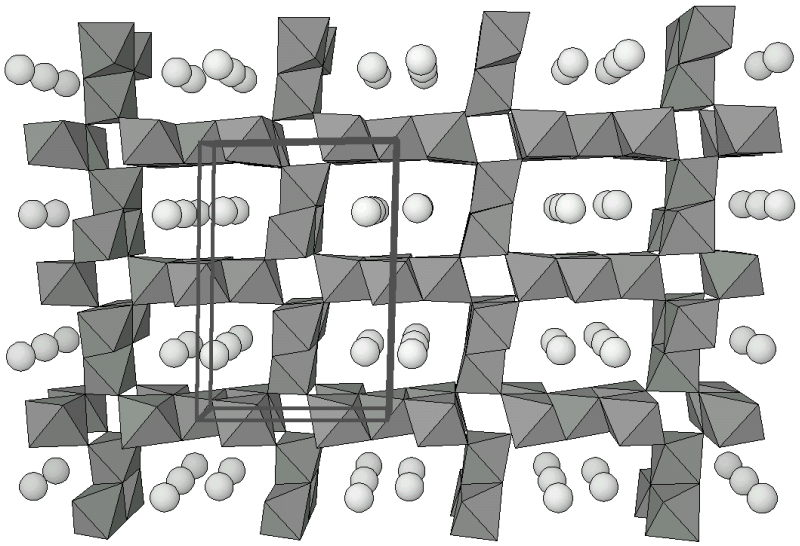

(a)

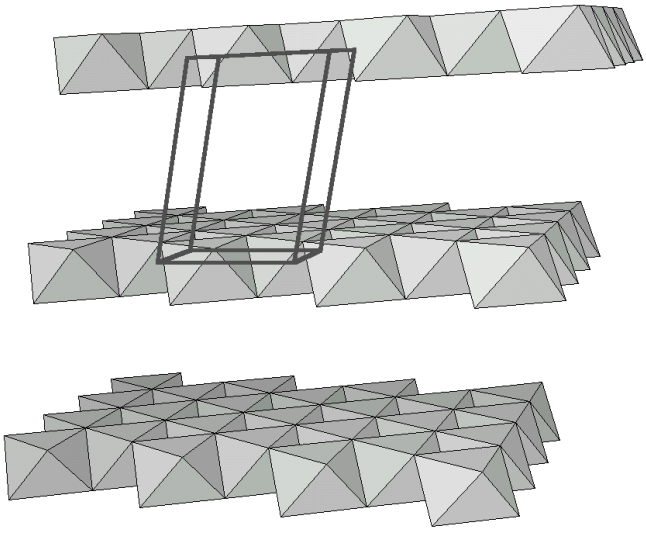

(b)

Figure 1

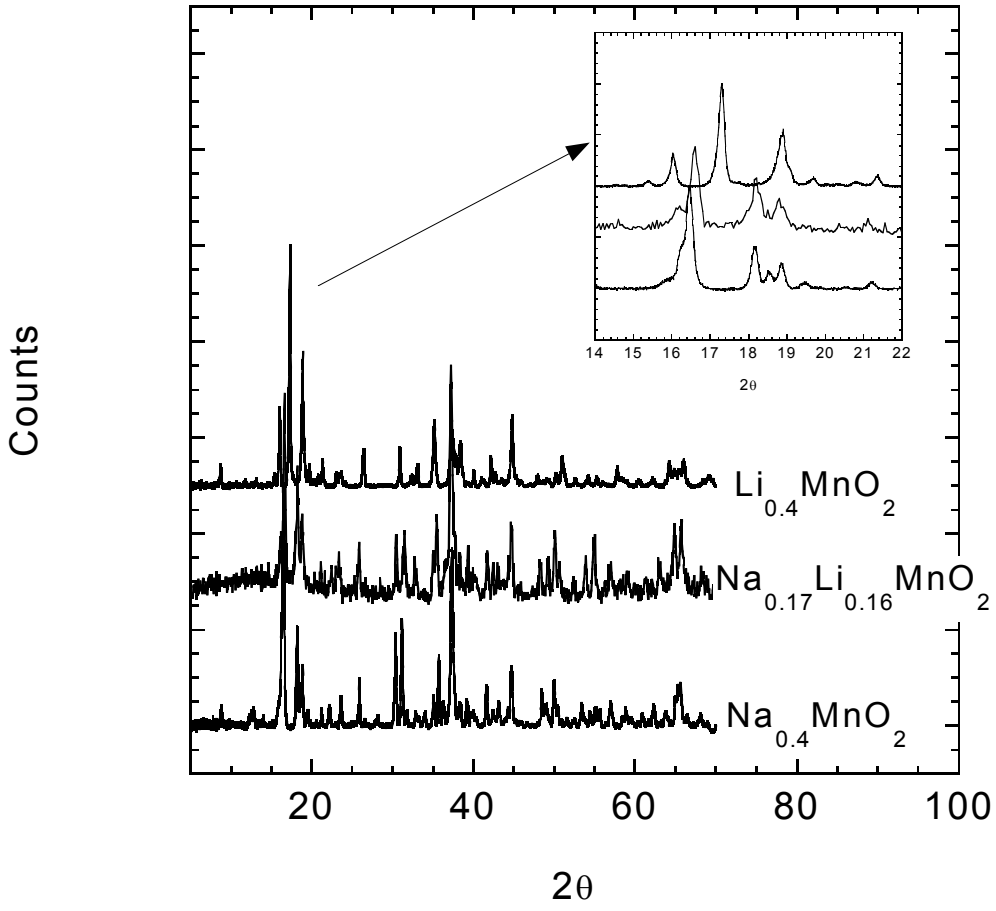
Counts
Li0.4MnO2
Na0.17Li0.16MnO2
Na0.4MnO2
20
40
60
80
100
2θ
14
15
16
17
18
19
20
21
22
2θ

Figure 2

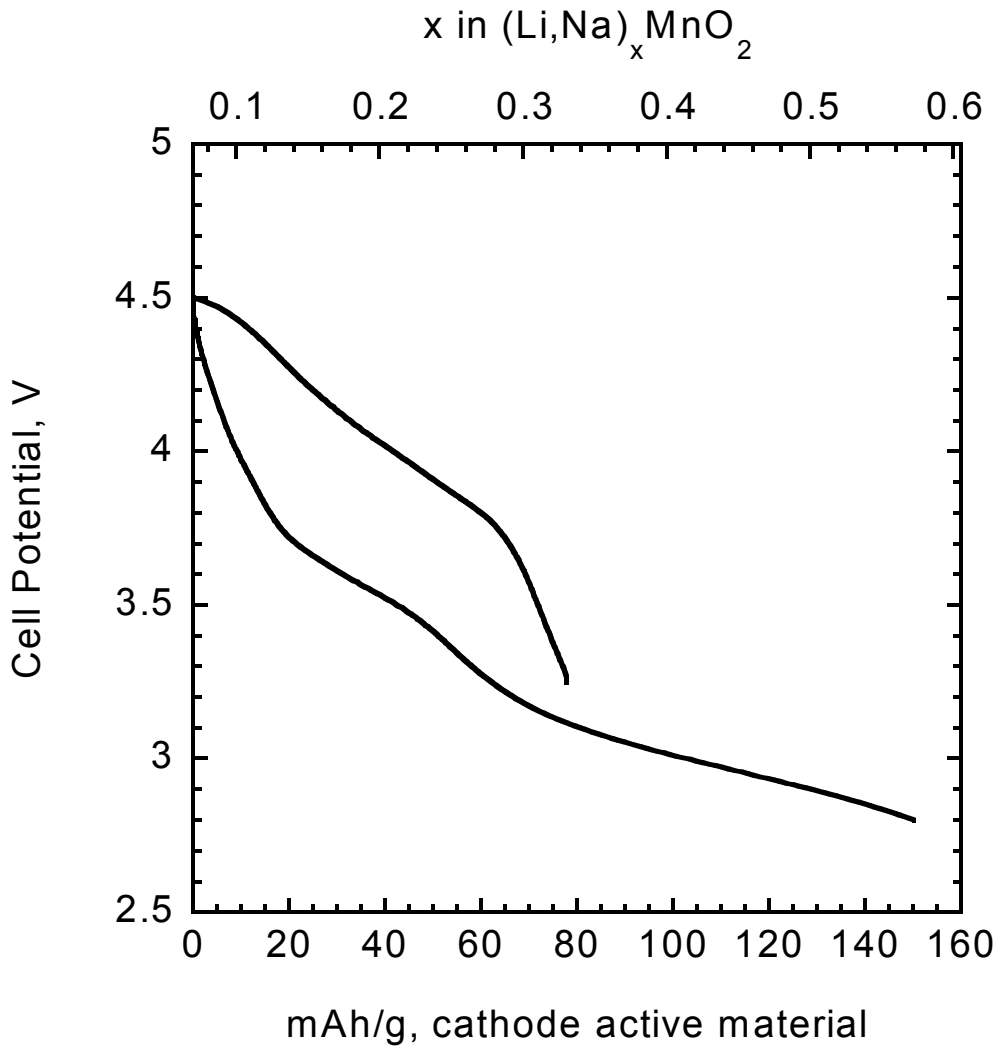
x in (Li,Na)xMnO2
0.1
0.2
0.3
0.4
0.5
0.6
5
4.5
4
3.5
3
2.5
Cell Potential, V
0
20
40
60
80
100
120
140
160
mAh/g, cathode active material

Figure 3

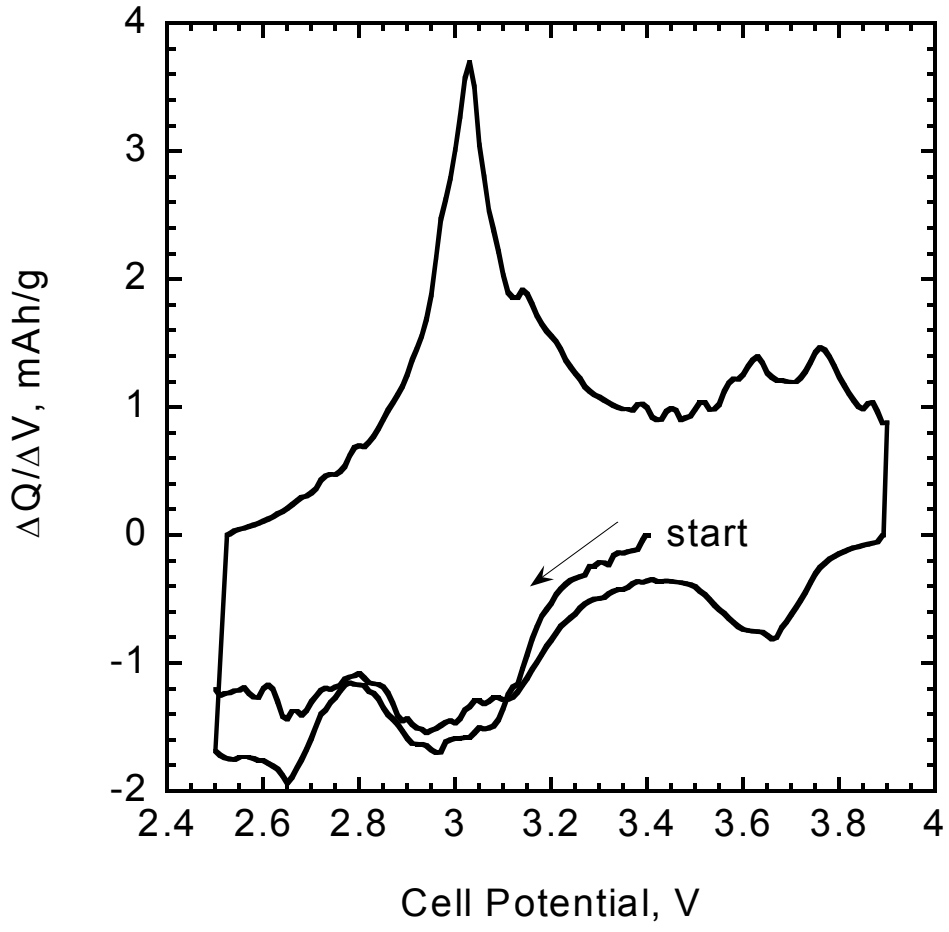
4
3
2
1
0
-1
-2
ΔQ/ΔV, mAh/g
start
2.4
2.6
2.8
3
3.2
3.4
3.6
3.8
4
Cell Potential, V

Figure 4.

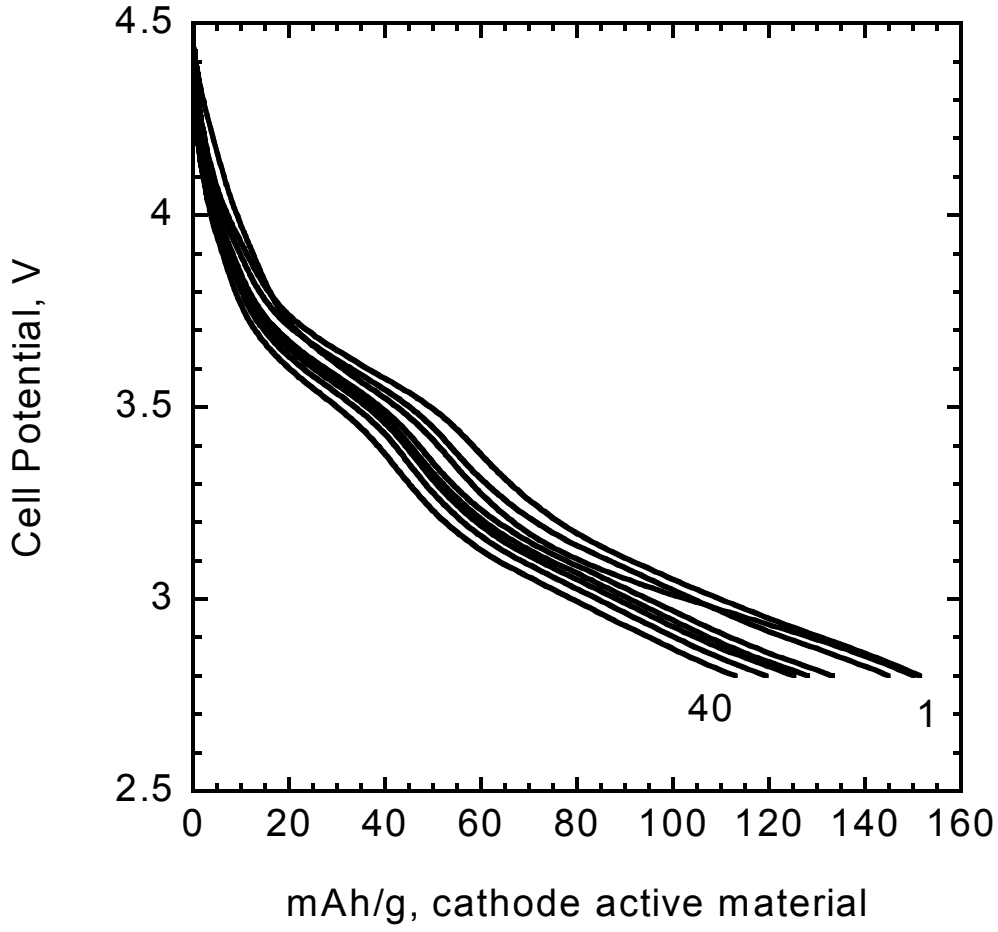
4.5
4
3.5
3
2.5
Cell Potential, V
0
20
40
60
80
100
120
140
160
mAh/g, cathode active material
40
1

Figure 5

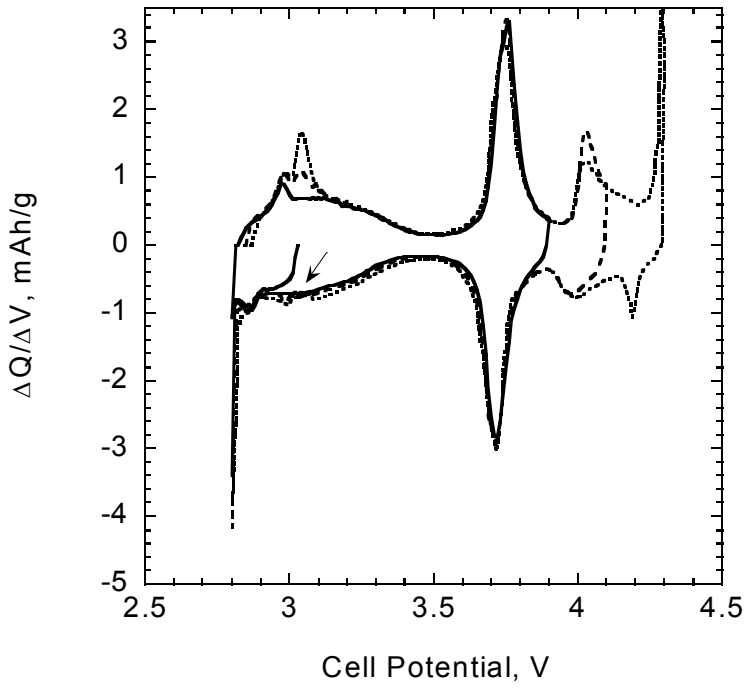
3
2
1
0
-1
-2
-3
-4
-5
2.5
3
3.5
4
4.5
ΔQ/ΔV, mAh/g
Cell Potential, V

(a)

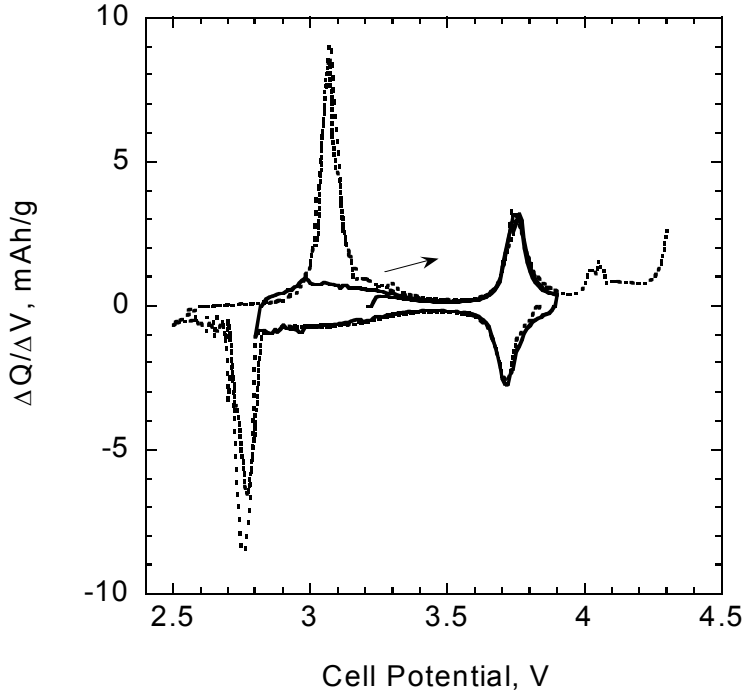
10
5
0
-5
-10
2.5
3
3.5
4
4.5
ΔQ/ΔV, mAh/g
Cell Potential, V

(b)

Figure 6.

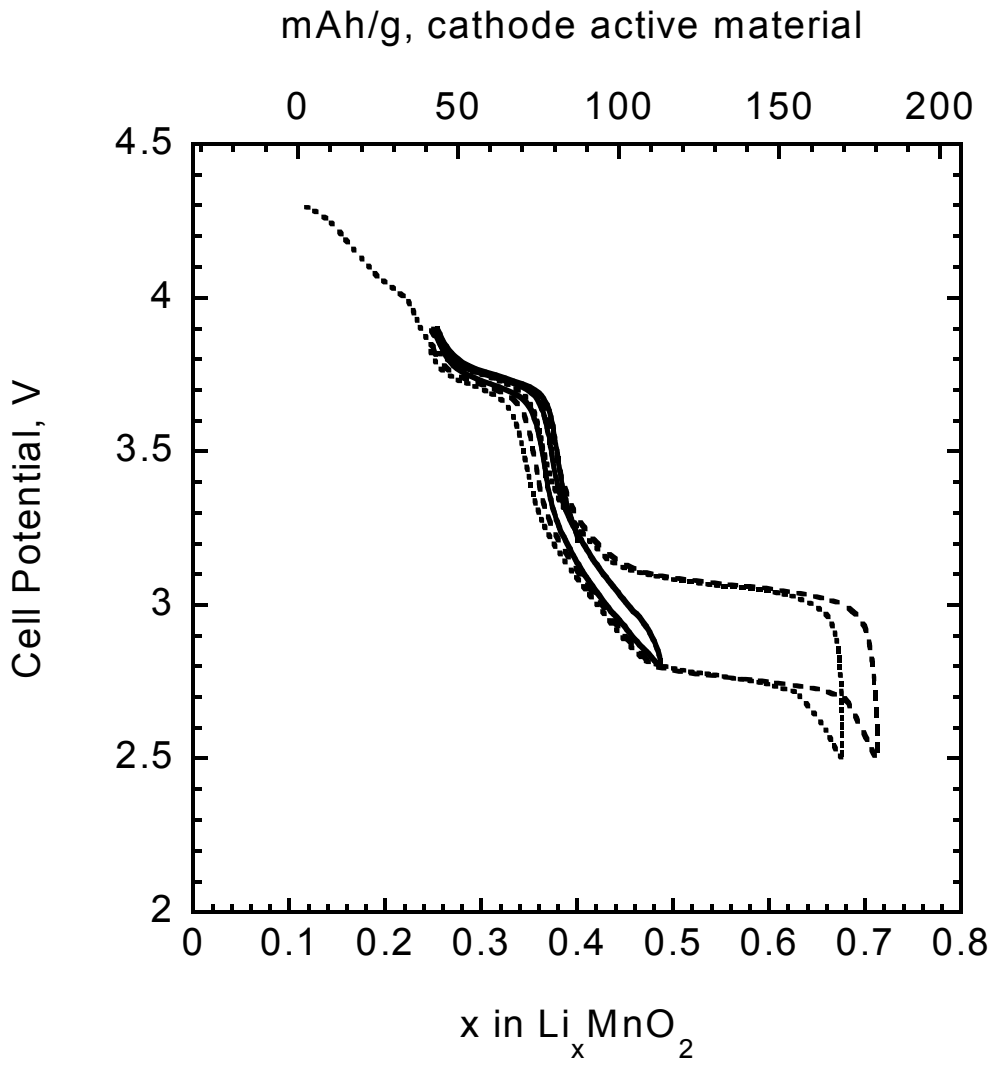
mAh/g, cathode active material
0
50
100
150
200
4.5
4
3.5
3
2.5
2
Cell Potential, V
0
0.1
0.2
0.3
0.4
0.5
0.6
0.7
0.8
x in Li x MnO 2

Figure 7.

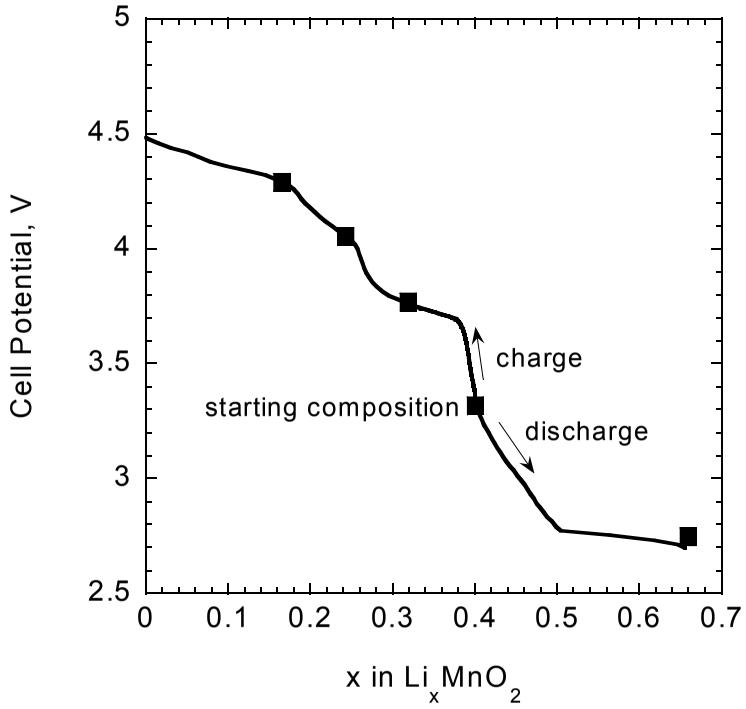
Cell Potential, V
5
4.5
4
3.5
3
2.5
0
0.1
0.2
0.3
0.4
0.5
0.6
0.7
x in Li$_x$MnO$_2$
charge
starting composition
discharge

(a)

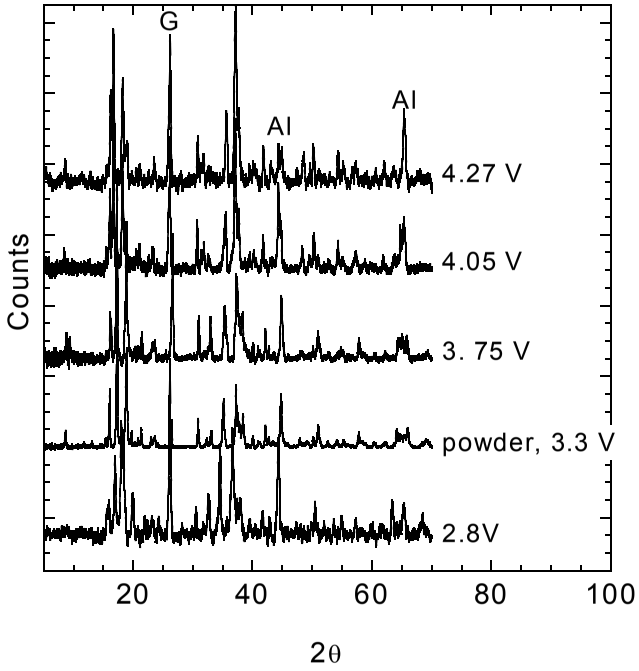
Counts
G
Al
Al
4.27 V
4.05 V
3. 75 V
powder, 3.3 V
2.8V
20
40
60
80
100
2θ

(b)

Figure 8.

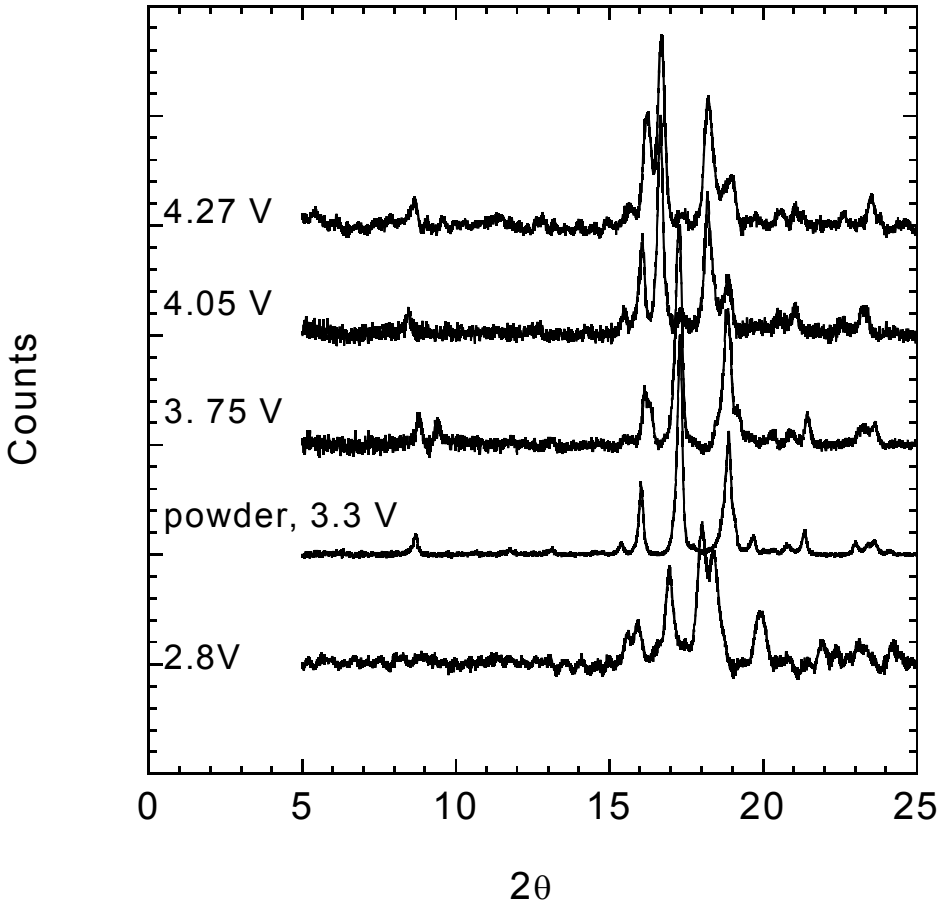

Figure 9.

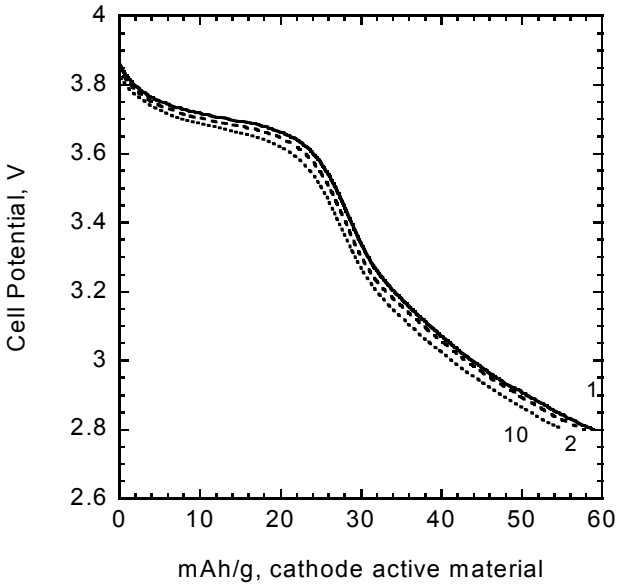
Cell Potential, V
mAh/g, cathode active material
1
2
10

(a)

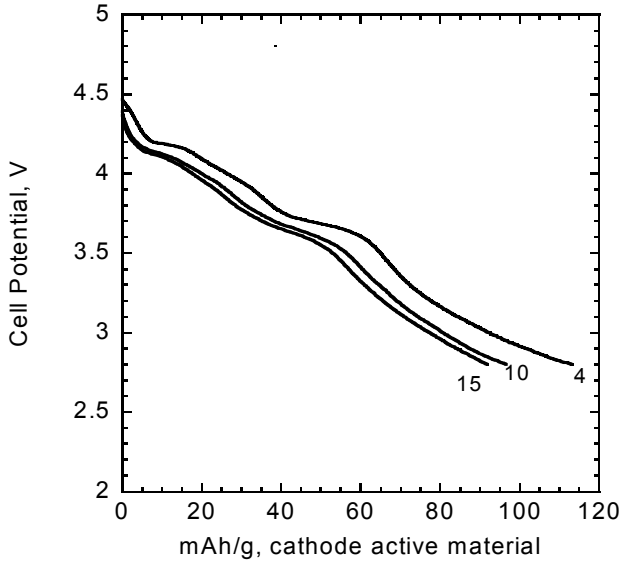
Cell Potential, V
mAh/g, cathode active material
4
10
15

(b)

Figure 10.